frontiers | Frontiers in Physics

TYPE Original Research
PUBLISHED 01 December 2022
DOI 10.3389/fphy.2022.1066166

OPEN ACCESS

EDITED BY
Houkun Liang,
Sichuan University, China

REVIEWED BY
Xiaohui Li,
Shaanxi Normal University, China
Chujun Zhao,
Hunan University, China

*CORRESPONDENCE
Chen Wei,
cwei@uestc.edu.cn

SPECIALTY SECTION
This article was submitted to Optics and Photonics, a section of the journal Frontiers in Physics

RECEIVED 10 October 2022
ACCEPTED 18 November 2022
PUBLISHED 01 December 2022

CITATION
Zheng L, Sun F, Zhou H, Gao A, Liu W, Wang D, Wei C and Liu Y (2022), MIL-68(Al) and MIL-68(Fe) as broadband optical modulators for Q-switching fiber lasers operating at 2 and 2.9 μm. *Front. Phys.* 10:1066166. doi: 10.3389/fphy.2022.1066166

MIL-68(Al) and MIL-68(Fe) as broadband optical modulators for Q-switching fiber lasers operating at 2 and 2.9 μm

Le Zheng, Fanxi Sun, Hongrong Zhou, Ang Gao, Wenshu Liu, Dongsheng Wang, Chen Wei* and Yong Liu

School of Optoelectronic Science and Engineering, State Key Laboratory of Electronic Thin Films and Integrated Devices, University of Electronic Science and Technology of China (UESTC), Chengdu, China

We investigated 2 and 2.9 μm mid-infrared fiber lasers passively Q-switched by MIL-68(Al) and MIL-68(Fe), which were fabricated *via* the hydrothermal method. The modulation depth of MIL-68(Al) was found to be 9.12% at 1.99 μm. And the modulation depths of MIL-68(Fe) were found to be 18.89% and 15.79% at 1.99 μm and 2.87 μm, respectively. We report Q-switching pulse generation in both Tm^{3+}-doped and Ho^{3+}/Pr^{3+} co-doped fiber lasers by using the as-prepared MIL-68 (M, M = Al^{3+}, Fe^{3+}) as SAs. The center wavelengths were at 1.99 μm and 2.87 μm, respectively. These results indicate that MIL-68(M) has wideband nonlinear optical properties and promising application prospects in the field of optical modulators at 2- and 2.9-μm mid-infrared waveband. Work clearly accessible to a broad readership.

KEYWORDS

metal-organic frameworks, mid-infrared, pulsed fiber lasers, saturable absorber, MIL-68(Al), MIL-68(Fe)

Introduction

Mid-infrared pulsed fiber laser sources operating in the 2 and 3 μm spectral regions have remained a research hotspot attributed to their numerous applications in remote sensing, spectroscopy, free-space communications, and laser surgery [1–6]. Compared with actively modulated pulsed lasers, the passively modulated ones with saturable absorbers, such as passively Q-switched and passively mode-locked lasers, show the merits of low cost and simple structure without the requirement of high-voltage and RF drivers. In recent years, a variety of nanomaterials with unique electronic structures and significant nonlinear optical properties have drawn great attention due to their wide application in areas such as all-optical switches, photo-detectors, optical modulators and pulsed lasers [7–13]. Among them, two-dimensional (2D) nanomaterials, such as graphene, transition metal dichalcogenides (TMDs), black phosphorus (BP), topological insulators (TIs), bismuthene, MXene, and antimonene, with their 2D planar structure, ultrafast carrier dynamics and broadband absorption, have been widely investigated for

their excellent optical and optoelectronic properties [14, 15]. Especially in the field of pulsed fiber lasers, they have been successfully used as saturable absorbers for short pulse generation at various wavebands, driving the development of pulsed fiber lasers [16–32]. Some binary chalcogenides (SnS, PbS, and In_2S_3) have also shown saturable absorption properties [33–35]. However, they still have limitations. For example, the weak absorption of graphene makes it difficult to ensure a suitable modulation depth for pulse generation [36]. TMDs is mainly used to implement pulsed fiber lasers in the visible spectral range while the large direct band gap limits their application in the mid-infrared region [20, 37]. Although BP is the most stable allotrope of the phosphorus, it is prone to oxidation and reacts more strongly when it was exposed to water, limiting its application due to the poor stability [38]. In recent years, metal-organic frameworks materials (MOFs), microcrystalline porous materials self-assembled from metal ions or clusters and organic ligands, have received increasing attention and research due to their remarkable advantages including large surface area, ordered reticular structure, excellent electrical conductivity, excellent optical transparency [39]. MOFs have been extensively applied in the fields of chemical sensing, catalytic, gas storage, molecular magnets and nonlinear optical [40–44]. In recent years, the use of MOFs and their derived nanomaterials as saturable absorbers in fiber laser pulse generation is also being gradually investigated, such as nickel-p-benzenedicarboxylic acid MOFs (Ni-MOFs) [45, 46], zeolitic imidazolate framework-8 (ZIF-8) [47], NiO-MOF [48], rGO-Co_3O_4 [49].

As a typical kind of MOF, MIL-68(M) (M = Fe^{3+}, Al^{3+}, In^{3+} etc.) are built from the infinite chains of corner-sharing metal-centered octahedral $MO_4(OH)_2$ linked through hydroxyl groups and terephthalate ligands [50, 51]. The organic ligand (terephthalate) and metal atoms of MIL-68(M) are orderly assembled in a layer-by-layer manner, exhibiting 2D crystalline structure. MIL-68(M) has both triangular and hexagonal pores, demonstrating high chemical stability, high surface area and sufficient thermal stability up to 500°C [51–54]. The outstanding properties make them attractive. Currently, it has been shown that MIL-68(Al) and MIL-68(Fe) have good nonlinear optical properties at 2.8 μm [55]. However, the investigation on the nonlinear properties in other wavelength bands is still lacking.

Herein, MIL-68(Al) and MIL-68(Fe) were prepared by hydrothermal method and we investigated their nonlinear optical properties in 2 μm and 2.9 μm regions. Furthermore, pulse generation was achieved in both Tm^{3+}-doped and Ho^{3+}/Pr^{3+} co-doped fiber lasers by using MIL-68(Al) and MIL-68(Fe) as SAs, operating at 2 μm and 2.9 μm, respectively. These results indicate that MIL-68(Al) and MIL-68(Fe) can be developed as promising broadband SAs for mid-infrared pulses generation.

Preparation and characterization of MIL-68(Al) and MIL-68(Fe)

The synthesis of MIL-68(Al) and MIL-68(Fe) is the same as the literature [55]. The morphology of MIL-68(Al) crystals was observed by transmission electron microscopy (TEM), as shown in Figure 1A. According to the TEM image, the prepared MIL-68(Al) are clusters of needlelike crystals with different lengths [56]. Figure 1B shows the XRD pattern of MIL-68(Al) crystals. All the characteristic peaks of the MIL-68(Al) material are similar to those previous literatures [57, 58].

Similarly, the as-prepared MIL-68 (Fe) sample was also characterized. Figure 2A shows the TEM image and the size of the as-synthesized MIL-68(Fe) is about 1–3 μm. As shown in Figure 2B, the positions of the typical peaks of the XRD pattern matched well with the previous work, indicating that the crystal lattice parameters (cell length and angle) are the same but differ in relative intensity. However, the relative intensities are different influenced by the meritocratic orientation [59].

Figure 3 shows the measurement setup of the nonlinear absorptions. A self-made laser which generates pulse duration of 1.42 ps at 1.99 μm was used as one of the laser sources, as shown in Figure 3A. An optical output coupler with 50:50 fiber-pigtailed was used to simultaneously detect the reference signal and absorption. MIL-68(Al) or MIL-68(Fe) were coated on a CaF_2 window plate (F1) and the F2 was an uncoated CaF_2 window plate. Two detectors (D1 and D2) were used to measure the average powers. In addition, we used a homemade mode-locked fiber laser operating at 2.87 μm as the other laser source. The repetition rate is 18.39 MHz and a pulse duration is ~20 ps. The balanced twin detector system was elaborated in Ref. [19], as shown in Figure 3B.

The parameters of the SAs were fitted with the following formula: $\boldsymbol{R(I) = 1 - \Delta R \cdot exp(-\frac{I}{I_{sat}}) - R_{ns}}$, where $\boldsymbol{R(I)}$ indicates the reflectivity, $\boldsymbol{\Delta R}$ is the modulation depth, $\boldsymbol{I}$ is the incident peak intensity, $\boldsymbol{I_{sat}}$ is the saturation peak intensity and $\boldsymbol{R_{ns}}$ represents the non-saturable loss [19]. Figure 4A shows the experimental results. The modulation depth, non-saturable loss, and saturation peak intensity of MIL-68(Al) were fitted to be 9.12%, 41.47%, and 0.3468 GW/cm^2. As shown in Figures 4B,C, the modulation depth, non-saturable loss, and saturation peak intensity of MIL-68(Fe) were fitted to be 18.89%/15.79%, 35.51%/52.47%, and 0.2198 GW/cm^2/0.0044 GW/cm^2 under 1.99 μm and 2.87 μm laser irradiation, respectively.

Tm: Fiber Q-switched laser

Experiment setup

The experimental setup of the passively Q-switched Tm^{3+}-doped fiber laser is depicted in Figure 5. An all-fiber-integrated ring cavity configuration was adopted. The pump source was a

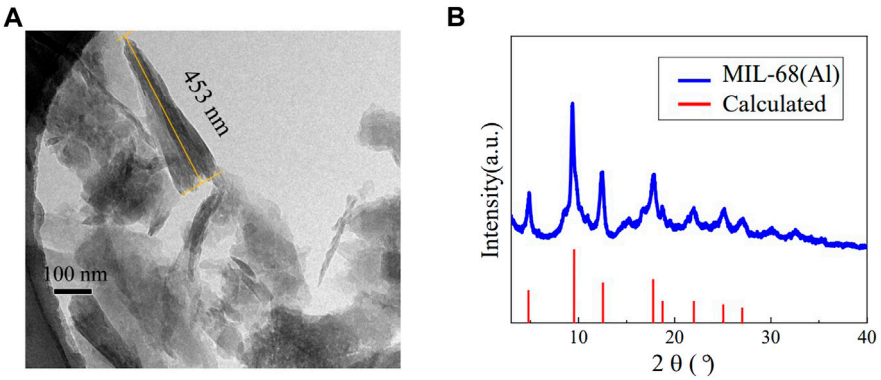

FIGURE 1
(A) TEM image of MIL-68(Al) with a 100 nm scale; **(B)** XRD pattern of as-synthesized MIL-68(Al).

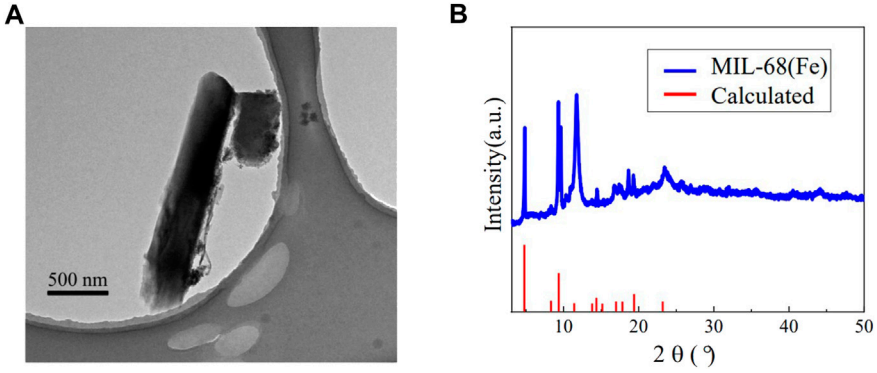

FIGURE 2
(A) TEM image of MIL-68(Fe) with a 500 nm scale; **(B)** XRD pattern of as-synthesized MIL-68(Fe).

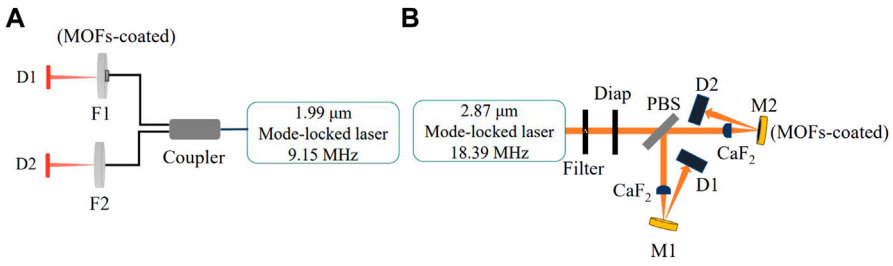

FIGURE 3
Nonlinear absorption experimental setup, **(A)** at 1.99 μm, **(B)** at 2.87 μm.

12 W commercial 793 nm diode laser (BWT). The gain fiber was a 5.8 m double-clad Tm^{3+}-doped fiber (Coractive, 4 dB/m absorption at790 nm) which has a diameter of 128 μm and a numerical aperture (NA) of 0.22. The gain fiber was pumped *via* a (1 + 1) × 1 pump combiner. The fiber circulator guaranteed the one-way light propagation in the ring cavity with definite light propagation direction (1→2→3). In addition, the port-2 pigtail of the circulator was vertically cut to the fiber axis and

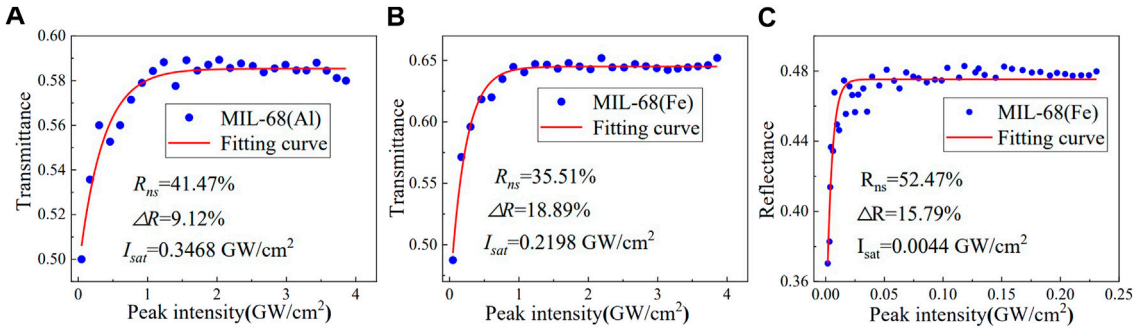

FIGURE 4
Transmittance and reflectance of the samples as a function of pulse peak intensity. **(A)** MIL-68(Al) at 1.99 μm; **(B)** MIL-68(Fe) at 1.99 μm; **(C)** MIL-68(Fe) at 2.87 μm.

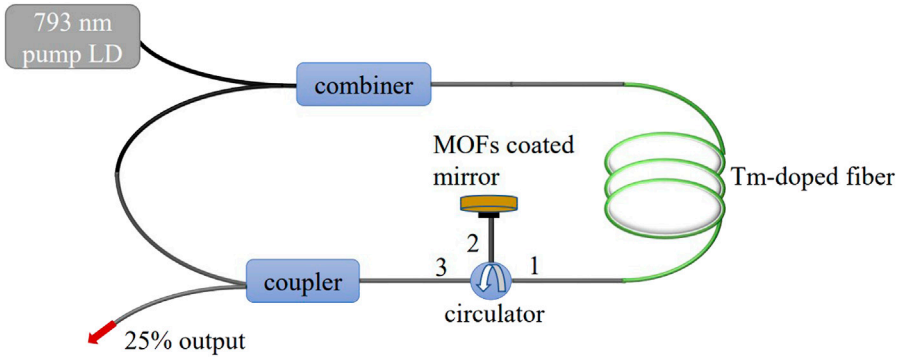

FIGURE 5
Experimental setup of the passively Q-switched Tm^{3+}-doped fiber laser based on the MOFs SA.

positioned closely to the gold mirror coated with MOFs for optical modulation and feedback. A 25% port of a 25/75 fiber coupler was used to output the laser from the cavity. The average output power was measured with a power meter (Laserpoint). A 350-MHz-bandwidth digital oscilloscope was used to record the pulse trains and waveforms. The spectral profiles of output pulses were monitored by an optical spectrum analyzer (Yokogawa AQ6375, Japan).

Results and discussion

The MIL-68(Al)-based passively Q-switched operation self-stared when the pump power was increased to 2.06 W, as shown in Figure 6A. A repetition rate of 38.81 kHz and a pulse duration of 5.73 μs were obtained. As the pump power gradually increased to 2.57 W, the pulse sequence maintained a stable Q-switched state with a repetition rate of 42.44 kHz and the minimum pulse duration of 2.13 μs. Once the pump power exceeded 2.57 W, the pulse trains started to grow erratic and then faded away. Nevertheless, stable Q-switching operation could be recaptured when the pump power was decreased, demonstrating that the MIL-68(Al) was not damaged by the photothermal effect [19, 32]. The high optical damage threshold of MIL-68(Al) was also confirmed [55]. The Q-switched output power increased from 1.37 mW to 3.08 mW and the maximum pulse energy was 0.073 μJ, as displayed in Figure 6B. Accordingly, the highest peak power was calculated to be 0.034 W. The inset shows that the center wavelength of the pulsed laser is 1988.5 nm. The repetition rate increased from 38.81 kHz to 42.44 kHz as the pump power increased, as displayed in Figure 6C. Specifically, the pulse duration decreased from 5.73 μs to 2.13 μs. As shown in the inset, the signal-to-noise ratio (SNR) of 41.1 dB was measured at the frequency of 42.44 kHz, indicating a stable Q-switched operation.

When MIL-68(Al) was replaced with MIL-68(Fe) in the same experimental setup, the MIL-68(Fe)-based passively Q-switched operation self-started as the pump power raised to 1.59 W, as

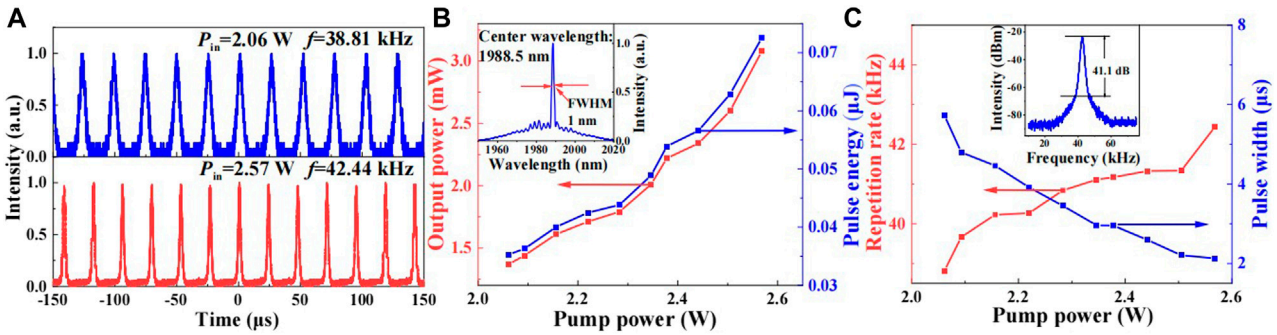

FIGURE 6
(A) Q-switched pulse trains at the launched pump power of 2.06 W and 2.57 W; **(B)** Output power and single-pulse energy as functions of the pump power, inset: optical spectra of the Q-switched pulses; **(C)** repetition rate and pulse width as functions of the pump power, inset: RF spectra of the Q-switched pulses.

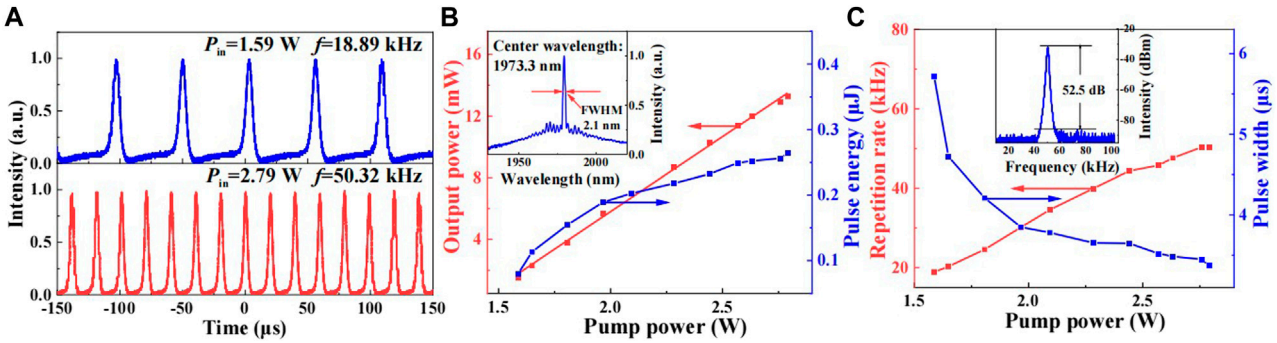

FIGURE 7
(A) Q-switched pulse trains at the launched pump power of 1.59 W and 2.79 W; **(B)** Output power and single-pulse energy as functions of the pump power, inset: optical spectra of the Q-switched pulses; **(C)** repetition rate and pulse width as functions of the pump power, inset: RF spectra of the Q-switched pulses.

shown in Figure 7A. The repetition rate was 18.89 kHz. Stable Q-switching operation without any adjustment was sustained until the launched pump power of 2.79 W. The repetition rate and pulse duration were 50.32 kHz and 3.37 μs, respectively. With further increasing the launched pump power, the Q-switching began unstable and then disappeared. When we reduced the pump power to less than 2.79 W again, stable Q-switched operation could be observed again. As the launched pump power rising from 1.59 W to 2.79 W, the Q-switched output power and pulse energy both increased, as shown in Figure 7B. The maximum output power of 13.3 mW and the maximum pulse energy of 0.26 μJ were received. Accordingly, the highest peak power of 0.078 W was obtained. The center wavelength was 1973.3 nm, as shown in the inset. Figure 7C shows the variation of Q-switched pulses over the same pump range. The repetition rate raised from 18.89 kHz to 50.32 kHz while the pulse duration decreased from 5.72 μs to 3.37 μs. The measured signal-to-noise ratio (SNR) was 52.5 dB at the frequency of 50.32 kHz, indicating a stable Q-switched operation.

Mode-locked operation of the two fiber lasers were not observed in our experiments. This may be related to the parameters of SAs and/or the current laser resonator design. By comparing selected all-fiber Q-switched lasers operating in the 2 μm region in Table 1, the minimum pulse width of MIL-68(Al) in this work is better and the maximum pulse energy of MIL-68(Fe) measured in this system is higher than most of materials reported previously [20–22, 30, 31]. Compared with traditional SESAM, MOFs has the characteristics of simple manufacturing process and compared with low-dimensional materials like BP and TMDs, MOFs exhibits better physiochemical stability with high laser damage threshold, as well as the high temperature stability (~500°C). In addition, the pulse width obtained by using MIL-68(Al) as SA is narrower and

TABLE 1 Comparison of this work with other selected 2D-materials for the two-micron region.

Gain medium	SA	Wavelength (nm)	Output power (mW)	Pulse duration (μs)	Repetition rate (kHz)	Pulse energy (nJ)	Peak power (mW)	References
Tm^{3+}	$MoSe_2$	1924	~0.9	5.5	21.8	42	—	[20]
Tm^{3+}	$MoWSe_2$	1964	240	2.4	61.5	85	—	[21]
Tm^{3+} Ho^{3+}	$MoWS_2$	1983	—	2.78	36.3	86.4	31.1	[22]
Tm^{3+}	Ti_3AlC_2	1980.79	1.43	2.72	32.57	45.23	15.49	[30]
Ho^{3+}	Nb_2C-PVA	2079.5	1.2	4.4	20.5	56.6	—	[31]
Tm^{3+}	MoS_2	2032	47.3	1.76	48.1	~100	—	[37]
Tm^{3+}	MIL-68(Al)	1988.5	3.08	2.13	42.44	73	34	This work
Tm^{3+}	MIL-68(Fe)	1973.3	13.3	3.37	50.32	26	78	This work

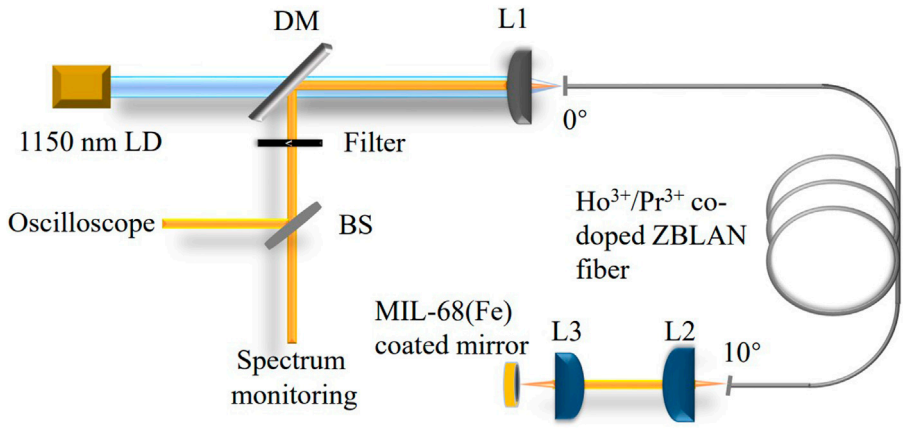

FIGURE 8
Experimental setup of the passively Q-switched Ho^{3+}/Pr^{3+}-doped ZBLAN fiber laser based on the MOFs SA.

the pulse energy is higher compared to the one when using MIL-68(Fe) as SA, while the average output power and peak power obtained by using MIL-68(Fe) as SA are both higher compared to the ones when using MIL-68(Al) as SA.

Ho^{3+}/Pr^{3+}: Fiber Q-switched laser

Experiment setup

We have also studied the optical performance in the 3-μm waveband of MIL-68(Fe). We established the MIL-68(Fe) SAs enabled passively Q-switched mid-infrared fiber laser. Figure 8 shows the experimental setup of the passively Q-switched fiber laser based on MIL-68(Fe). The pump light was a commercial laser diodes (LD) (Eagleyard Photonics) operating at 1,150 nm. A 5.5 m long Ho^{3+}/Pr^{3+} co-doped ZBLAN fiber (FiberLabs) was used as the gain fiber. The core diameter is 10 μm and numerical aperture (NA) is 0.2. The front end of fiber was vertically cut to the fiber axis to provide a 4% feedback. A dichroic mirror (DM) which has a high reflectivity at 2.8 μm and high transparency at 1,150 nm was 45°placed to be used as the output coupler. An anti-reflection CaF_2 plano-convex lens (L1: f = 20 mm) was employed to collimate the laser beam. The coupling efficiency was estimated to be 82% [30]. The output light beam from the angle-cleaved fiber end was collimated and focused onto the gold mirror coated through MIL-68(Fe) with a pair of ZnSe objective lens (L2: f = 12 mm, L3: f = 6 mm).

Results and discussion

The fiber laser started Q-switching operation when the incident pump power was increased to 0.46 W, as shown in

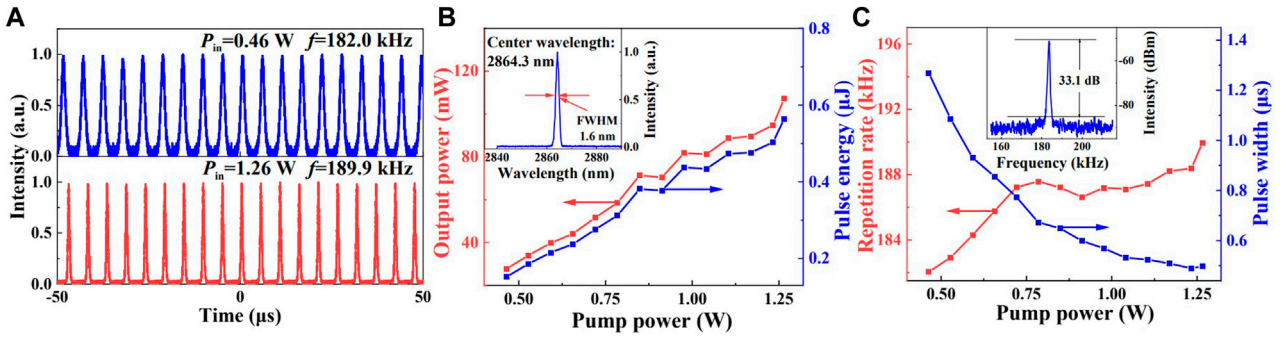

FIGURE 9
(A) Q-switched pulse trains at the launched pump power of 0.46 W and 1.26 W; **(B)** Output power and single-pulse energy as functions of the pump power, inset: optical spectra of the Q-switched pulses; **(C)** repetition rate and pulse width as functions of the pump power, inset: RF spectra of the Q-switched pulses.

TABLE 2 Comparison of this work with other selected 2D-materials for the three-micron region.

Gain medium	SA	Wavelength (nm)	Output power (mW)	Pulse duration (μs)	Repetition rate (kHz)	Pulse energy (nJ)	Peak power (W)	References
Er^{3+}	graphene	2780.0	62.0	2.90	37	1,670	0.58	[17]
Er^{3+}	BP	2771.5	18.4	3.32	22.2	820	—	[25]
Er^{3+}	MXene-Ti_3C_2Tx	2786.2	1,090	1,040	78.12	13,930	19,130	[29]
Ho^{3+}/Pr^{3+}	$PtSe_2$	2865.0	93.0	0.62	238.1	389	0.63	[19]
Ho^{3+}/Pr^{3+}	WS_2	2865.7	48.4	1.63	131.6	420	0.21	[23]
Ho^{3+}/Pr^{3+}	antimonene	2868.0	112.3	1.74	156.2	720	0.41	[32]
Ho^{3+}/Pr^{3+}	MIL-68(Fe)	2864.3	107.2	0.497	189.9	560	1.14	This work

Figure 9A. The repetition rate and pulse duration were 182.0 kHz and 1.26 μs. The Q-switching operation can be maintained until the pump power of 1.26 W. The shortest pulse width of 497 ns was obtained with a repetition rate of 189.9 kHz. Figure 9B shows the Q-switched average output power and pulse energy over the same incident pump power. The output power increased linearly with the pump power and the maximum output power was 107.2 mW. The maximum pulse energy of 0.56 μJ and peak power of 1.14 W were obtained. The inset shows the Q-switched pulse spectrum and the center wavelength locates at 2,864.3 nm. The full width at half maxima (FWHM) was 1.6 nm. The repetition rate raised from 182.0 kHz to 189.9 kHz while the pulse width decreased from 1.26 μs to 497 ns, as displayed in Figure 9C. The radio-frequency (RF) spectrum with a signal-to-noise ratio (SNR) of 33.1 dB was measured at the repetition rate of 189.9 kHz, as shown in the inset of Figure 9C.

In contrast to the output characteristics of 2.9 μm Q-switched Ho^{3+} and Ho^{3+}/Po^{3+} co-doped fiber lasers modulated by the typical 2D materials, a stable passive Q-switched laser with a short pulse width of 497 ns, which is the shortest one, as far as we know, was investigated based on a novel MIL-68(Fe)-SA. As can be seen in Table 2, The generated pulse peak power manifested the advantages compared with materials like graphene [17], $PtSe_2$ [19], WS_2 [23], antimonene [32] etc. In addition, the MIL-68(Al) and MIL-68(Fe) SAs used in our experiments were stored in the thermostat for two to 3 months and then the Q-switched laser experiments were repeated. Stable Q-switching pulses can still be achieved, although the pulse performances are slightly different at a given pump power. The results show that MIL-68(Al) and MIL-68(Fe) are SA materials with long-term stability in the mid-infrared spectral range.

Conclusion

In summary, MIL-68(Al) and MIL-68(Fe) were fabricated by hydrothermal method and the saturable absorption

properties were characterized under 1.99 μm and 2.87 μm laser irradiation, respectively. We developed Tm^{3+}-doped fiber laser operating at 1988.5 nm using MIL-68(Al) as SA. In addition, we developed MIL-68(Fe) Q-switched Tm^{3+}-doped and Ho^{3+}/Pr^{3+} co-doped fiber lasers, operating at 1.98 μm and 2,864.3 nm, with pulse durations of 3.37 μs and 467 ns, respectively. Our results show the potential of MIL-68 (M, M = Al^{3+}, Fe^{3+}) with excellent optical properties and extraordinary opportunities for application in mid-infrared spectral region.

Data availability statement

The original contributions presented in the study are included in the article/supplementary materials, further inquiries can be directed to the corresponding author.

Author contributions

All authors listed have made a substantial, direct, and intellectual contribution to the work and approved it for publication.

Funding

National Natural Science Foundation of China (61875033 and 61421002); Science and Technology Planning Project of Sichuan Province (2022NSFSC1790 and 2020ZHCG0087). Fundamental Research Funds for the Central Universities (YGX2019J051).

Conflict of interest

The authors declare that the research was conducted in the absence of any commercial or financial relationships that could be construed as a potential conflict of interest.

Publisher's note

All claims expressed in this article are solely those of the authors and do not necessarily represent those of their affiliated organizations, or those of the publisher, the editors and the reviewers. Any product that may be evaluated in this article, or claim that may be made by its manufacturer, is not guaranteed or endorsed by the publisher.

References

1. Godard A. Infrared (2–12 μm) solid-state laser sources: A review. *Comptes Rendus Physique* (2007) 8(10):1100–28. doi:10.1016/j.crhy.2007.09.010

2. Boulnois JL. Photophysical processes in recent medical laser developments: A review. *Laser Med Sci* (1986) 1(1):47–66. doi:10.1007/BF02030737

3. Ebrahim-Zadeh M, Sorokina IT. *Mid-infrared coherent sources and applications NATO science for peace and security series B: Physics and biophysics*. Springer (2008). p. 467–6122.

4. Skorczakowski M, Swiderski J, Pichola W, Nyga P, Zajac A, Maciejewska M, et al. Mid-infrared Q-switched Er: YAG laser for medical applications. *Laser Phys Lett* (2010) 7(7):498–504. doi:10.1002/lapl.201010019

5. Halmer D, Thelen S, Hering P, Murtz M. Online monitoring of ethane traces in exhaled breath with a difference frequency generation spectrometer. *Appl Phys B* (2006) 85(2):437–43. doi:10.1007/s00340-006-2288-9

6. Scherer JJ, Paul JB, Jost HJ, Fischer ML. Mid-IR difference frequency laser-based sensors for ambient CH_4, CO, and N_2O monitoring. *Appl Phys B* (2013) 110(2):271–7. doi:10.1007/s00340-012-5244-x

7. Sun Z, Martinez A, Wang F. Optical modulators with 2D layered materials. *Nat Photon* (2016) 10:227–38. doi:10.1038/nphoton.2016.15

8. Xia F, Mueller T, Lin Y, Valdes-Garcia A, Avouris P. Ultrafast graphene photodetector. *Nat Nanotechnol* (2009) 4:839–43. doi:10.1038/nnano.2009.292

9. Zhang X, Ouyang H, Miao R, Sui Y, Hao H, Tang Y, et al. Anisotropic nonlinear optical properties of a SnSe flake and a novel perspective for the application of all-optical switching. *Adv Opt Mater* (2019) 7(18):1900631. doi:10.1002/adom.201900631

10. Keller U. Recent developments in compact ultrafast lasers. *Nature* (2003) 424:831–8. doi:10.1038/nature01938

11. Mu H, Wang Z, Yuan J, Xiao S, Chen C, Chen Y, et al. Graphene–Bi_2Te_3 heterostructure as saturable absorber for short pulse generation. *ACS Photon* (2015) 2:832–41. doi:10.1021/acsphotonics.5b00193

12. Li X, Xu W, Wang Y, Zhang X, Hui Z, Zhang H, et al. Optical-intensity modulators with PbTe thermoelectric nanopowders for ultrafast photonics. *Appl Mater Today* (2022) 28(8):101546. doi:10.1016/j.apmt.2022.101546

13. Zhang C, Li X, Chen E, Liu H, Shum P, Chen X. Hydrazone organics with third-order nonlinear optical effect for femtosecond pulse generation and control in the L-band. *Opt Laser Technology* (2022) 151(9):108016. doi:10.1016/j.optlastec.2022.108016

14. Ma C, Wang C, Gao B, Adams J, Wu G, Zhang H. Recent progress in ultrafast lasers based on 2D materials as a saturable absorber. *Appl Phys Rev* (2019) 6(4):041304. doi:10.1063/1.5099188

15. Jiang T, Yin K, Wang C, You J, Ouyang H, Miao R, et al. Ultrafast fiber lasers mode-locked by two-dimensional materials: Review and prospect. *Photon Res* (2020) 8(1):78–90. doi:10.1364/PRJ.8.000078

16. Zhang M, Kelleher EJR, Torrisi F, Sun Z, Hasan T, Popa D, et al. Tm-doped fiber laser mode-locked by graphene-polymer composite. *Opt Express* (2012) 20(22):25077–84. doi:10.1364/OE.20.025077

17. Wei C, Zhu XH, Wang F, Xu Y, Balakrishnan K, Song F, et al. Graphene Q-switched 2.78 μm Er^{3+}-doped fluoride fiber laser. *Opt Lett* (2013) 38:3233–6. doi:10.1364/OL.38.003233

18. Tiu ZC, Ooi SI, Guo J, Zhang H, Ahmad H. Review: Application of transition metal dichalcogenide in pulsed fiber laser system. *Mater Res Express* (2019) 6:082004. doi:10.1088/2053-1591/ab2257

19. Wei C, Chi H, Jiang S, Zheng L, Zhang H, Liu Y. Long-term stable platinum diselenide for nanosecond pulse generation in a 3-μm mid-infrared fiber laser. *Opt Express* (2020) 28(22):33758–66. doi:10.1364/OE.410110

20. Woodward RI, Howe RCT, Runcorn TH, Hu G, Torrisi F, Kelleher EJR, et al. Wideband saturable absorption in few-layer molybdenum diselenide ($MoSe_2$) for Q-switching Yb-Er- and Tm-doped fiber lasers. *Opt Express* (2015) 23:20051. doi:10.1364/oe.23.020051

21. Ahmad H, Reduan SA, Aidit SN, Yusoff N, Maah MJ, Ismail MF, et al. Ternary $MoWSe_2$ alloy saturable absorber for Passively Q-switched thulium-doped fiber laser with silver-nanoparticle film as the saturable absorber for operation at 2.0 μm Yb-Er- and Tm-doped fiber laser. *Opt Commun* (2019) 437:355–62. doi:10.1016/j.optcom.2019.01.009

22. Ahmad H, Sharbirin AS, Ismail MF. Molybdenum tungsten disulphide ($MoWS_2$) as a saturable absorber for a passively Q-switched thulium/holmium-co doped fiber laser. *J Mod Opt* (2019) 66:1163–71. doi:10.1080/09500340.2019.1609612

23. Wei C, Luo H, Zhang H, Li C, Xie J, Li J. Passively Q-switched mid-infrared fluoride fiber laser around 3 μm using a tungsten disulfide (WS_2) saturable absorber. *Laser Phys Lett* (2016) 13:105108. doi:10.1088/1612-2011/13/10/105108

24. Chen Y, Jiang G, Chen S, Guo Z, Yu X, Zhao C, et al. Mechanically exfoliated black phosphorus as a new saturable absorber for both Q-switching and mode-locking laser operation. *Opt Express* (2015) 23(10):12823–33. doi:10.1364/OE.23.012823

25. Qin ZP, Xie GQ, Ma JG, Yuan P, Qian LJ. 2.8 μm all-fiber Q-switched and mode-locked lasers with black phosphorus. *Photon Res* (2018) 6:1074–8. doi:10.1364/PRJ.6.001074

26. Dou Z, Song Y, Tian J, Liu J, Yu Z, Fang X. Mode-locked ytterbium-doped fiber laser based on topological insulator: Bi_2Se_3. *Bi_2se3 Opt Express* (2014) 22(20):24055–61. doi:10.1364/OE.22.024055

27. Guo B, Wang SH, Wu ZX, Wang ZX, Wang DH, Huang H, et al. Sub-200 fs soliton mode-locked fiber laser based on bismuthene saturable absorber. *Opt Express* (2018) 26(18):22750–60. doi:10.1364/OE.26.022750

28. Wu Q, Jin X, Chen S, Jiang X, Hu Y, Jiang Q, et al. MXene-based saturable absorber for femtosecond mode-locked fiber lasers. *Opt Express* (2019) 27(7): 10159–70. doi:10.1364/OE.27.010159

29. Wei C, Zhou L, Wang D, Chi H, Huang H, Zhang H, et al. MXene-Ti_3C_2Tx for watt-level high-efficiency pulse generation in a 2.8 μm mid-infrared fiber laser. *Photon Res* (2020) 8(6):972–7. doi:10.1364/PRJ.388930

30. Ahmad H, Kamely AA, Yusoff N, Bayang L, Samion MZ. Generation of Q-switched pulses in Thulium doped and Thulium/Holmium-co-doped fiber lasers using MAX phase (Ti_3AlC_2). *Sci Rep* (2020) 10:9233. doi:10.1038/s41598-020-66141-3

31. Ahmad H, Ismail NN, Aidit SN, Reduan S, Samion M, Yusoff N. 2.08 μm Q-switched holmium fiber laser using niobium carbide-polyvinyl alcohol (Nb_2C-PVA) as a saturable absorber. *Opt Commun* (2021) 490:126888. doi:10.1016/j.optcom.2021.126888

32. Luo HY, Tian XL, Gao Y, Wei RF, Li JF, Qiu JR, et al. Antimonene: A long-term stable two-dimensional saturable absorption material under ambient conditions for the mid-infrared spectral region. *Photon Res* (2018) 6:900–7. doi:10.1364/PRJ.6.000900

33. Xie Z, Zhang F, Liang Z, Fan T, Li Z, Jiang X, et al. Revealing of the ultrafast third-order nonlinear optical response and enabled photonic application in two-dimensional tin sulfide. *Photon Res* (2019) 7(5):494–502. doi:10.1364/PRJ.7.000494

34. Liu X, Li X, Tang Y, Zhang S. PbS nanoparticles saturable absorber for ultrafast pulse generation in 2-μm fiber laser. *Opt Lett* (2020) 45(1):161–4. doi:10.1364/OL.45.000161

35. Ma X, Chen W, Tong L, Liu S, Dai W, Ye S, et al. In_2S_3-based saturable absorber for passively harmonic mode-locking in 2μm region. *Opt Laser Technology* (2022) 145:107476. doi:10.1016/j.optlastec.2021.107476

36. Martinez A, Sun Z. Nanotube and graphene saturable absorbers for fibre lasers. *Nat Photon* (2013) 7(11):842–5. doi:10.1038/nphoton.2013.304

37. Luo Z, Huang Y, Zhong M, Li Y, Wu J, Xu B, et al. 1-1.5-and 2-μm fiber lasers Q-switched by a broadband few-layer MoS_2 saturable absorber. *J Lightwave Technol* (2014) 32:4679–86. doi:10.1109/JLT.2014.2362147

38. Favron A, Gaufrès E, Fossard F, Phaneuf-L'Heureux A, Tang NYW, Lévesque PL, et al. Photooxidation and quantum confinement effects in exfoliated black phosphorus. *Nat Mater* (2015) 14(8):826–32. doi:10.1038/nmat4299

39. Yaghi OM, O'Keeffe M, Ockwig NW, Chae HK, Eddaoudi M, Kim J. Reticular synthesis and the design of new materials. *Nature* (2003) 423(6914):705–14. doi:10.1038/nature01650

40. Qu F, Jiang H, Yang M. Designed formation through a metal organic framework route of $ZnO/ZnCo_2O_4$ hollow core–shell nanocages with enhanced gas sensing properties. *Nanoscale* (2016) 8:16349–56. doi:10.1039/C6NR05187A

41. Furukawa H, Cordova K, O'Keeffe M, Yaghi O. The chemistry and applications of metal-organic frameworks. *Science* (2013) 341(6149):1230444. doi:10.1126/science.1230444

42. Kuppler RJ, Timmons DJ, Fang QR, Li JR, Makal TA, Young MD, et al. Potential applications of metal-organic frameworks. *Coord Chem Rev* (2009) 253(23):3042–66. doi:10.1016/j.ccr.2009.05.019

43. Silva P, Vilela S, Tome J, Almeida PF. Multifunctional metal–organic frameworks: From academia to industrial applications. *Chem Soc Rev* (2015) 44(19):6774–803. doi:10.1039/c5cs00307e

44. Evans OR, Lin W. Crystal engineering of NLO materials based on metal-organic coordination networks. *Acc Chem Res* (2002) 35(7):511–22. doi:10.1021/ar0001012

45. Jiang X, Zhang L, Liu S, Zhang Y, He Z, Li W, et al. Ultrathin metal-organic framework: An emerging broadband nonlinear optical material for ultrafast photonics. *Adv Opt Mater* (2018) 6(16):1800561. doi:10.1002/adom.201800561

46. Zhang Q, Jiang X, Zhang M, Jin X, Zhang H, Zheng Z. Wideband saturable absorption in metal–organic frameworks (MOFs) for mode-locking Er- and Tm-doped fiber lasers. *Nanoscale* (2020) 12(7):4586–90. doi:10.1039/C9NR09330C

47. Dong L, Chu H, Li Y, Zhao S, Li D. Broadband optical nonlinearity of zeolitic imidazolate framework-8 (ZIF-8) for ultrafast photonics. *J Mater Chem C Mater* (2021) 9(28):8912–9. doi:10.1039/D1TC01665B

48. Zhang C, Liu J, Gao Y, Li X, Lu H, Wang Y, et al. Porous nickel oxide micron polyhedral particles for high-performance ultrafast photonics. *Opt Laser Technology* (2022) 146(40):107546. doi:10.1016/j.optlastec.2021.107546

49. Li X, An M, Li G, Han Y, Guo P, Chen E, et al. MOF-derived porous dodecahedron rGO-Co_3O_4 for robust pulse generation. *Adv Mater Inter* (2022) 9(5):2101933. doi:10.1002/admi.202101933

50. Barthelet K, Marrot J, Ferey G, Riou D. III(OH){O_2C–C_6H_4–CO_2}.(HO_2C–C_6H_4–CO_2H)x(DMF)y(H_2O)z (or MIL-68), a new vanadocarboxylate with a large pore hybrid topology : Reticular synthesis with infinite inorganic building blocks? *Chem Commun* (2004) 5:520–1. doi:10.1039/b312589k

51. Volkringer C, Meddouri M, Loiseau T, Guillou N, Marrot J, Ferey G, et al. The kagome topology of the gallium and indium metal-organic framework types with a MIL-68 structure: Synthesis, XRD, solid-state NMR characterizations, and hydrogen adsorption. *Inorg Chem* (2008) 47(24):11892–901. doi:10.1021/ic801624v

52. Yang Q, Vaesen S, Vishnuvarthan M, Ragon F, Serre C, Vimont A, et al. Probing the adsorption performance of the hybrid porous MIL-68(Al): A synergic combination of experimental and modelling tools. *J Mater Chem* (2012) 22(10): 10210–20. doi:10.1039/c2jm15609a

53. Fateeva A, Horcajada P, Devic T, Serre C, Marrot J, Grenèche JM, et al. Synthesis, structure, characterization, and redox properties of the porous MIL-68(Fe) solid. *Eur J Inorg Chem* (2010) 2010(24):3789–94. doi:10.1002/ejic.201000486

54. Seoane B, Sebastian V, Tellez C, Coronas J. Crystallization in THF: The possibility of one-pot synthesis of mixed matrix membranes containing MOF MIL-68(Al). *CrystEngComm* (2013) 15(45):9483–90. doi:10.1039/c3ce40847g

55. Zheng L, Wei C, Zhou H, Sun F, Gao A, Wang D, et al. Mid-infrared optical switches enabled by metal-organic frameworks for compact high-power nanosecond laser sources at 3 μm. *Opt Express* (2022) 30(8):12409–19. doi:10.1364/OE.455854

56. Jiang Y, Zhang B, Li J, Sun Y, Wang X, Ma P, et al. One-step fabrication of hydrophilic MIL-68(Al)/Chitosan-coated melamine sponge for vortex-assisted solid-phase extraction of parabens in water samples. *Talanta* (2021) 1(224): 121799. doi:10.1016/j.talanta.2020.121799

57. Tehrani MS, Zare-Dorabei R. Competitive removal of hazardous dyes from aqueous solution by MIL-68(Al): Derivative spectrophotometric method and response surface methodology approach. *Spectrochimica Acta A: Mol Biomol Spectrosc* (2016) 160:8–18. doi:10.1016/j.saa.2016.02.002

58. Embrechts H, Kriesten M, Ermer M, Peukert W, Hartmann M, Distaso M. *In situ* Raman and FTIR spectroscopic study on the formation of the isomers MIL-68(Al) and MIL-53(Al). *RSC Adv* (2020) 10:7336–48. doi:10.1039/c9ra09968a

59. Jing FF, Liang RW, Xiong JH, Chen R, Zhang SY, Li YH, et al. MIL-68(Fe) as an efficient visible-light-driven photocatalyst for the treatment of a simulated wastewater contain Cr(VI) and Malachite Green. *Appl Catal B: Environ* (2017) 206:9–15. doi:10.1016/j.apcatb.2016.12.070